

UC San Diego

UC San Diego Previously Published Works

Title

Defects of the Lamina Cribrosa in Eyes with Localized Retinal Nerve Fiber Layer Loss

Permalink

<https://escholarship.org/uc/item/11p3s0s8>

Journal

Ophthalmology, 121(1)

ISSN

0161-6420

Authors

Tatham, Andrew J
Miki, Atsuya
Weinreb, Robert N
et al.

Publication Date

2014

DOI

10.1016/j.opthta.2013.08.018

Peer reviewed

Published in final edited form as:

Ophthalmology. 2014 January ; 121(1): 110–118. doi:10.1016/j.ophtha.2013.08.018.

Defects of the lamina cribrosa in eyes with localized retinal nerve fiber layer loss

Andrew J. Tatham, FRCOphth¹, Atsuya Miki, M.D., Ph.D.¹, Robert N. Weinreb, M.D.¹, Linda M. Zangwill, Ph.D.¹, and Felipe A. Medeiros, M.D., Ph.D.¹

¹Hamilton Glaucoma Center and Department of Ophthalmology, University of California, San Diego

Abstract

Objective—To determine whether focal abnormalities of the lamina cribrosa (LC) are present in glaucomatous eyes with localized retinal nerve fiber layer (RNFL) defects.

Design—Cross-sectional observational study.

Participants—20 eyes of 14 subjects with localized RNFL defects detected by masked grading of stereophotographs and 40 eyes of 25 age-matched healthy subjects recruited from the Diagnostic Innovations in Glaucoma Study (DIGS) at the University of California, San Diego.

Methods—All eyes had stereoscopic optic disc photography and in vivo LC imaging using enhanced depth optical coherence tomography (EDI-OCT). Two masked graders identified focal LC defects defined by a standardized protocol using 48 radial scan EDI-OCT images. The Kappa coefficient was calculated as a measure of the reliability of interobserver agreement.

Main Outcome Measures—The number of focal LC defects and the relationship between the location of LC defects and the location of localized RNFL defects.

Results—15 of 20 eyes with a localized RNFL defect (75%) had at least one LC defect compared to only 1 of 40 healthy eyes (3%). 13 eyes with localized RNFL defects had 1 LC defect, 1 eye had 2 LC defects and 1 eye had 3 LC defects. The largest area LC defect was present in a radial line EDI-OCT scan corresponding to a localized RNFL defect in 13/15 (87%) of eyes. There was good agreement between graders as to whether an eye had a LC defect (Kappa=0.87, 95% CI 0.73–1.00, P<0.001) and the location of the largest defect (Kappa=0.72, 95% CI 0.44–1.00, P<0.001).

© 2013 American Academy of Ophthalmology, Inc. Published by Elsevier Inc. All rights reserved.

Corresponding Author: Felipe A. Medeiros, M.D., Ph.D., Hamilton Glaucoma Center, University of California, San Diego, 9500 Gilman Drive, La Jolla, CA 92093-0946, fmedeiros@glaucoma.ucsd.edu.

Publisher's Disclaimer: This is a PDF file of an unedited manuscript that has been accepted for publication. As a service to our customers we are providing this early version of the manuscript. The manuscript will undergo copyediting, typesetting, and review of the resulting proof before it is published in its final citable form. Please note that during the production process errors may be discovered which could affect the content, and all legal disclaimers that apply to the journal pertain.

Financial Disclosure(s):

The author(s) have made the following disclosure(s):

A.J.T. – none

A.M. – consultant for Nidek

L.M.Z. – research support (equipment) from Carl-Zeiss Meditec, and Heidelberg Engineering

R.N.W. – research support from Carl Zeiss-Meditec, Heidelberg Engineering, Optovue, Kowa; consultant for Carl Zeiss-Meditec, Nidek and Topcon.

F.A.M. – financial support from Carl-Zeiss Meditec, and Heidelberg Engineering

Conclusions—Focal defects of the lamina cribrosa were frequently visible in glaucomatous eyes with localized RNFL defects. Focal abnormalities of the LC may be associated with focal retinal nerve fiber damage.

The lamina cribrosa (LC) is a meshwork of connective tissue through which retinal ganglion cell axons pass as they exit the eye through the scleral canal.^{1,2} The collagenous beams of the LC provide mechanical support for the nerve fiber bundles, while nutritional support is provided by extracellular matrix components, glial cells such as astrocytes, blood vessels within lamina beams, and axonal transport.^{3–5} The LC is subject to intraocular pressure (IOP)-related stress and strain, and is implicated as the putative site of retinal ganglion cell damage in glaucoma.^{5–8}

Histological studies in humans and animals have shown that eyes with glaucoma or raised IOP often have deformities of the LC.^{7–11} Abnormalities include posterior lamina displacement, lamina thinning, pore deformities and lamina defects. Damage to the LC may also be seen clinically, for example, as an enlargement of lamina pores or as an acquired pit of the optic nerve. Burgoyne and colleagues proposed that deformation of the LC is a manifestation of IOP-related connective tissue damage and that axonal damage is likely to occur concurrently to LC damage.⁵ Damage to the LC is also likely to increase the risk of further axonal damage due to increased exposure to compressive or shearing forces,^{5,12} or due to damage to supporting cells^{4,5} and withdrawal of axonal support.

Regional differences in the LC may make specific portions of the optic nerve particularly susceptible to neural loss.^{3,13–15} For example, LC pores are larger, and connective tissue septae thinner, at the superior and inferior poles of the optic nerve head.¹⁶ The lamina in these regions is likely to offer less structural support for retinal ganglion cell axons and less resistance to mechanical deformation. This may explain why there is preferential damage to the arcuate nerve fibers in glaucoma.^{15,17} Regional differences in the LC may also explain why glaucoma is often associated with localized neural losses, such as those leading to localized retinal nerve fiber layer (RNFL) defects.

Recently, structural deformities of the LC have been detected in vivo using enhanced depth imaging-optical coherence tomography (EDI-OCT).^{15,18–23} EDI-OCT can be used to provide high-resolution images of the deep optic nerve head structures including the LC and lamina pores.^{18,19} EDI allows clearer imaging of the LC beneath the scleral rim, neuroretinal rim and vascular structures than standard spectral domain OCT (SD-OCT).^{18,24}

The aim of this study was to use EDI-OCT to evaluate the LC of glaucomatous eyes with localized RNFL defects. The frequency and location of LC defects as well as their relationship to RNFL defects were assessed in glaucomatous eyes and compared to age-matched healthy controls.

Methods

Study Design

This was a cross-sectional study involving participants from the Diagnostic Innovations in Glaucoma Study (DIGS) (ClinicalTrials.gov identifier: NCT00221897). The DIGS is a prospective longitudinal study at the Hamilton Glaucoma Center at the Department of Ophthalmology, University of California, San Diego (UCSD) designed to evaluate optic nerve structure and visual function in glaucoma. Methodological details have been described previously.²⁵ Informed consent was obtained from all the participants, and the institutional review board approved all methods. All methods adhered to the tenets of the Declaration of

Helsinki for research involving human subjects. The study was Health Insurance Portability and Accountability Act (HIPAA) compliant.

Twenty glaucomatous eyes of 14 subjects with localized RNFL defects visible on masked grading of fundus stereophotographs were included, in addition to both eyes of 25 healthy subjects, matched for age using optimal bipartite matching (STATA, version 12; StataCorp LP). Eyes were classified as glaucomatous if they had repeatable (at least two consecutive) abnormal visual field test results, as defined by a pattern standard deviation with a P value < 5% and/or a glaucoma hemifield test result outside normal limits or presence of documented progressive optic disc damage based on masked grading of optic disc stereophotographs. 18 of 20 eyes (90%) with visible localized RNFL defects had a glaucomatous visual field defect and 2 of 20 eyes (10%) had progressive optic disc changes without a repeatable visual field defect. Healthy subjects were recruited from the general population through advertisements and from the staff and employees of UCSD. Healthy eyes had intraocular pressure of 21 mmHg or less with no history of increased intraocular pressure (IOP) and a normal standard automated perimetry (SAP) result.

At each visit, subjects underwent a comprehensive ophthalmologic examination including review of medical history, best-corrected visual acuity, slit-lamp biomicroscopy, IOP measurement, gonioscopy, dilated fundoscopic examination, stereoscopic optic disc photography, and SAP using the Swedish interactive threshold algorithm (SITA Standard 24-2, Carl Zeiss Meditec, Inc., Dublin, CA, USA). Only subjects with open angles on gonioscopy were included. Subjects were excluded if they presented with a best-corrected visual acuity of less than 20/40, spherical refraction outside ± 5.0 diopters and/or cylinder correction outside 3.0 diopters, or any other ocular or systemic disease that could affect the optic nerve or the visual field.

Stereophotograph Grading

All patients underwent simultaneous stereoscopic optic disc photography. Digital stereoscopic images were reviewed with a stereoscopic viewer (Screen-VU stereoscope, PS Mfg., Portland, Oregon, USA) by two or more experienced graders. Each grader was masked to the subject's identity and to the other test results. Details of the methodology employed to grade optic disc photographs at the UCSD Optic Disc Reading Center have been provided elsewhere.²⁵⁻²⁷ An identical protocol was used for optic disc grading in this study, only the photographs were digital. Eyes with localized RNFL defects were identified by at least 2 masked graders. RNFL defects were defined as defects wider than twice the width of an arteriole, extending from close to the disc margin into the parapapillary area, widening en route (i.e., wedge-shaped).²⁵ Slit defects narrower than the diameter of adjacent vessels were not included as they are frequently found in normal eyes.^{28,29}

Enhanced depth spectral domain OCT imaging

The Spectralis spectral-domain OCT (software version 5.4.7.0, Heidelberg Engineering, Dossenheim, Germany) was used to image the LC using the automated enhanced depth imaging (EDI) setting.^{18,19} Imaging was performed within 6 months of stereoscopic photography and SAP. Spectralis SD-OCT uses a dual-beam SD-OCT and a confocal laser-scanning ophthalmoscope that works by emitting a superluminescent diode light with a center wavelength of 870 nm and an infrared scan to simultaneously provide images of ocular microstructures. A real-time eye tracking system is incorporated that couples confocal laser scanning ophthalmoscope and SD-OCT scanners to adjust for eye movements and to ensure that the same location of the retina is scanned over time. The scans were obtained using the automatic real time (ART) mode, which uses multiple line acquisition to reduce noise. The number of ART repeat scans was set to average 9 images. The EDI scan

was obtained using 48 radial line B-scans centered on the optic disc (Figure 1), each at an angle of 3.75 degrees to the last. Each scan was 1024 pixels (6.1mm) in length and 496 pixels (1.9mm) in depth. RNFL thickness data was also obtained for each eye using 1536 A-scan points from a 3.45 mm circle scan centered on the optic disc.

Correct alignment of the optic disc photographs and EDI-OCT is important for investigation of the spatial relationship between LC and visible RNFL defects. The Spectralis SD-OCT uses fovea-to-disc (FoDi) alignment technology that generates a fovea to disc axis using the landmarks of the fovea and center of the optic disc on the SD-OCT infrared image. FoDi is used to automatically track and align circle scans to help overcome measurement errors due to changing head or eye position; however, this function is not enabled during EDI scanning. To overcome the problem of differences in alignment, image-processing software (GNU Image Manipulation Program, version 2.8, www.gimp.org. Accessed August 3, 2013) was used to calculate the angle of cyclotorsion between stereophotographs and EDI-OCT. The infrared EDI-OCT and SD-OCT images were superimposed on one of the stereophotograph pair and rotated to the point of best fit (Figure 1). The angle of cyclotorsion was used to calculate which of the 48 EDI-OCT radial line scans corresponded to the RNFL defect. Each of the 48 radial line EDI images was then examined independently, according to a standard protocol, by two graders (A.J.T. and A.M.) masked to the demographic and clinical details of the patient, including the presence or absence of glaucoma, and the location of any RNFL defects. All images were reviewed to ensure the scan was centered, that the signal strength was >15dB and that there were no artifacts. Eyes with poor quality images of the LC were excluded. A poor quality image was defined as a scan with less than 80% of the anterior LC visible within Bruch's membrane opening (BMO) in two or more of the 48 radial line scans (Figures 2 and 3). The BMO was identified manually in each image as the region between the terminations of Bruch's membrane at the optic nerve head.³⁰

A focal LC defect was defined as an anterior laminar surface irregularity violating the normal smooth curvilinear U- or W- shaped contour.¹⁵ To avoid false positives, defects needed to be greater than 100µm in diameter and 30µm in depth, and also be present in 2 neighboring radial line scans.¹⁵ Focal LC defects were classified as central or peripheral. Central defects were defined as defects within the BMO where the anterior LC was visible on either side of the defect (Figure 4A–C). The peripheral LC is often masked by the overlying scleral rim, therefore, peripheral defects were defined as defects where the anterior LC was visible on only one side of the defect (Figure 4D) and were further classified as within or peripheral to the BMO.

Focal LC defects were deemed to correspond to RNFL defects if they were present in axial line EDI-OCT scans transecting the visible stereophotograph RNFL defect. Localized stereophotograph RNFL defects and EDI-OCT LC defects were described as inferotemporal, superotemporal, inferonasal, superonasal, nasal or temporal depending on their location relative to the 6 sector SD-OCT peripapillary RNFL thickness classification map (Figure 3), after correction for cyclotorsion. If a defect involved more than one sector the defect was considered to affect the sector with the largest proportion of the defect. The largest area LC defect was determined using the Spectralis SD-OCT software version 5.4.7.0 calipers. If there was disagreement between graders regarding the presence or absence of LC defects in any of the 48 axial line scans, the EDI images were re-reviewed and a consensus grading obtained.

Statistical Analysis

The number of focal LC defects in eyes with localized RNFL defects was compared to the number of LC defects in healthy eyes and the number of defects in axial line EDI-OCT scans corresponding to the location of localized RNFL defects was compared to the number

of defects in axial line scans in regions without localized RNFL defects. Normality assumption was assessed by inspection of histograms and using Shapiro-Wilk tests. Student *t*-tests were used for group comparison for normally distributed variables, Wilcoxon rank-sum test for continuous non-normal variables and Fisher's exact test for categorical variables.

The Kappa coefficient for the graders' assessment of the presence or absence and the number of focal LC defects was calculated as a measure of the reliability of interobserver agreement.³¹ The Kappa coefficient adjusts the observed proportional agreement to take into account agreement which would be expected by chance, with Kappa=1 indicating perfect agreement and Kappa=0 no agreement.³² Confidence intervals for Kappa were obtained using 1000 bootstrap samples. All statistical analyses were performed with commercially available software (STATA, version 12; StataCorp LP). The α level (type I error) was set at 0.05.

Results

In 10 of the 50 healthy eyes (20%) there was poor visibility of the anterior LC (less than 80% of the anterior LC visible within the BMO) leaving a total of 40 eyes of 25 healthy subjects with good quality images. All 20 eyes of 14 patients with localized RNFL defects had good visibility of the anterior LC. The demographic characteristics of the subjects included in the study are summarized in Table 1.

Subjects with a localized RNFL defect had a mean (\pm standard deviation) age of 67.3 \pm 9.7 years compared to 67.6 \pm 10.1 years in healthy subjects ($P=0.946$). There was no significant difference in gender and race between healthy and glaucomatous subjects and there was no significant difference in central corneal thickness or axial length between healthy eyes and those with localized RNFL defects. In contrast, eyes with localized RNFL defects had significantly lower mean deviation ($P<0.001$) and mean RNFL thickness ($P<0.001$) than healthy eyes (Table 1). All eyes with localized RNFL defects had an IOP greater than 22mmHg on at least one prior occasion. The median maximum recorded IOP in eyes with localized RNFL defects was IOP was 31mmHg (interquartile range 29 to 32mmHg).

Location of retinal nerve fiber layer defects

Of the 20 eyes with localized RNFL defects, 18 had an inferotemporal RNFL defect, one had a superotemporal RNFL defect, and one eye had 2 non-contiguous RNFL defects, affecting the inferotemporal and superotemporal sectors.

Number of lamina cribrosa defects

Fifteen of 20 eyes with a localized RNFL defect (75%) had at least one focal LC defect detected. In contrast, there was only one healthy eye (of a 72 year old subject) with a focal LC defect. None of the healthy eyes with poor visibility of the LC had focal LC defects in the visible portion of the LC. An example of an eye without a LC defect is shown in Figure 2 and examples of eyes with LC defects are shown in Figures 3, 4 and 5. Thirteen eyes with localized RNFL defects had one LC defect, one eye had 2 LC defects and one eye had 3 LC defects, resulting in a total of 18 individual LC defects. There was excellent agreement between graders as to whether an eye had a LC defect or not (Kappa=0.87, 95% CI 0.73–1.00, $P<0.001$). With 25% of all eyes having a LC defect, a sample size of 60 eyes had a power of 90% to detect a Kappa of at least 0.75 as statistically significant ('kapssi' command, STATA, version 12; StataCorp).

There were 12 central LC defects (where the LC was visible on either side of the defect) (Figures 3A, 3B, 4A, 4B and 4C), and 6 peripheral LC defects (Figure 4D), including one eye with a LC defect peripheral to the BMO (Figure 5). There was good overall interobserver agreement regarding the number of LC defects detected (Kappa = 0.65, 95% CI = 0.64 to 0.76, $P < 0.001$). The diameter of the LC defects, measured at the anterior lamina surface, ranged from 101 to 186 μm . In eyes with localized RNFL defects, the mean (\pm standard deviation) RNFL thickness in sectors corresponding to a focal LC defect was 59.5 \pm 25.3 μm compared to 78.7 \pm 10.5 μm in sectors without a focal LC defect ($P = 0.002$). The single healthy eye with a focal LC defect had a global and sectorial SD-OCT RNFL thickness within normal limits. There was no significant difference in SAP mean deviation in eyes with localized RNFL defects with and without focal LC defects ($-4.8 \pm 2.8\text{dB}$ and $-4.7 \pm 3.3\text{dB}$ respectively; $P = 0.93$); however, eyes with focal LC defects had lower mean RNFL thickness (70.1 \pm 10.2 μm versus 81.0 \pm 11.0 μm , $P = 0.047$). There was also no significant difference in axial length and central corneal thickness in eyes with and without LC defects.

Location of lamina cribrosa defects

There were 13 focal LC defects in the inferotemporal sector, 3 defects in the superotemporal sector, 1 in the inferonasal sector and 1 in the superonasal sector. There were no focal LC defects detected in the nasal or temporal sectors. Fifteen of 18 focal LC defects in eyes with localized RNFL defects (83%) were in an EDI-OCT radial line scan transecting a localized RNFL defect. The largest focal LC defect in each eye was in an EDI-OCT radial line scan transecting a localized RNFL defect in 15 of 15 eyes (100%). In 13 eyes the largest focal LC defect was in the 50% of the EDI-OCT LC image closest to the visible RNFL defect. For example if the localized RNFL defect was inferotemporal, the LC defect was present in two consecutive radial line scans transecting the RNFL defect and in the inferotemporal half of these scans (Figures 4A and 4B). In 2 eyes a focal LC defect was present in radial line scans transecting a localized RNFL defect but was in the sector opposite the RNFL defect. For example, in an eye with an inferotemporal RNFL defect, a focal LC defect was present superotemporally. There was good inter-observer agreement regarding the location (RNFL thickness classification map sector) of the largest defect (Kappa=0.72, 95% CI 0.44–1.00, $P < 0.001$). Figures 3, 4 and 5 show examples of eyes with localized RNFL and LC defects and their spatial relation.

Discussion

This study demonstrates that focal defects of the LC can be detected in vivo using EDI-OCT in glaucomatous eyes with localized RNFL defects, with good inter-observer agreement. Fifteen out of 20 eyes with a localized RNFL defect (75%) had at least one focal LC defect detected. This result is similar to the findings of a previous EDI-OCT study, which found 34 of 38 eyes with glaucoma (89%) had a focal LC defect, and suggests that focal LC defects are common in glaucomatous eyes.¹⁵ In contrast, focal LC defects appear to be rare in healthy eyes. Kiumehr and colleagues found no focal LC defects in 92 healthy eyes, however, the healthy subjects were significantly younger than the glaucomatous patients.¹⁵ Structural changes such as RNFL thinning can occur with normal aging³³, therefore, it is feasible that LC defects might also develop with age. The present study included an age-matched healthy comparison group. Out of 40 healthy eyes, from subjects with a mean (\pm standard deviation) age of 68 \pm 10 years, there was only one focal LC defect detected, in a subject 72 years of age.

A second potentially important finding of the present study was that in eyes with localized RNFL defects, there was good spatial agreement between the location of the focal LC defects and the location of RNFL defects. In 13 of the 15 eyes (87%) with a localized RNFL

and a focal LC defect, the largest LC defect was in a radial line EDI-OCT scan and sector corresponding to the visible photographic RNFL defect. For example, Figure 4 shows 4 eyes with focal LC defects visible in radial line EDI-OCT scans in the same sector as localized RNFL defects visible on photography. In glaucomatous eyes, there were 3 LC defects detected on radial line EDI-OCT scans not transecting a visible localized RNFL defect. The SD-OCT RNFL thickness classification in the sector corresponding to the focal LC defect was outside normal limits in 2 of these cases and borderline in the third. Two further LC defects were present radial line scans transecting a localized RNFL defect but were located in the sector opposite, rather than adjacent to, the RNFL defect. In these eyes, the RNFL thickness classification was within normal limits in the sector adjacent to the focal LC defect. The LC defects were associated with significant RNFL thinning. In eyes with localized RNFL defects, the average RNFL thickness in SD-OCT sectors corresponding to focal LC defects was $60 \pm 15 \mu\text{m}$ which was significantly less than the average RNFL thickness of $79 \pm 11 \mu\text{m}$ in sectors without a focal LC defect ($P = 0.002$).

Although, it is not possible to establish whether focal LC defects are a cause or a consequence of the glaucomatous process, the results of this study suggest that localized structural defects of the LC might predispose to localized loss of retinal ganglion cell axons passing through the damaged sector. Axonal damage could occur in these circumstances due to loss of structural support from the lamina beams, due to direct injury from collapse of lamina beams, due to loss of nutrients derived from capillaries within the beams, due to impaired axonal flow, or from the loss of contact with supporting glial cells, such as astrocytes.^{4,13} It would follow that retinal ganglion cell axons in the region of lamina collapse would be most at risk of damage and therefore one would expect correlation between the location of LC defect and retinal ganglion cell loss. This concept is supported by the finding of a previous study, which showed correlation between the location of focal LC defects and the location of visual field loss.¹⁵

The greatest number of LC defects in the eyes included in this study was in the inferotemporal followed by superotemporal sectors. There were no focal LC defects detected in the nasal or temporal sectors. Primate studies have shown that IOP elevation may lead to mechanical failure of the LC and permanent connective tissue structural changes.^{5,8} The inferior and superior regions of the LC are known to contain larger pores and thinner connective tissue septae than the nasal and temporal sectors,^{13,34} which might render these areas of the LC particularly susceptible to deformation from IOP-related stresses and explain a susceptibility to focal defects in the LC.¹⁷ There is also some evidence that the number of focal LC defects is higher in eyes with more severe glaucoma. Kiumehr and colleagues found that the number of focal LC defects was correlated to mean deviation.¹⁵ Localized RNFL defects are often considered an early sign of glaucomatous damage^{35,36} and therefore one might expect a low number of focal LC defects in these eyes. In the present study, the eyes with localized RNFL defects had an average mean deviation of -4.8dB and an average of only 1 LC defect. This is similar to the number of LC defects found by Kiumehr and colleagues in eyes with a similar mean deviation.¹⁵ There was one eye in this study with 3 LC defects and this eye had a mean deviation of -11.18dB .

This study has several limitations. LC defects may have been missed due to poor visibility of the LC, especially in healthy eyes, 10 of which (10 of 50 eyes, 20%) were excluded due to poor visibility of the anterior LC. The detection of LC defects in healthy eyes may be more difficult than in glaucomatous eyes due to masking of the LC by thicker overlying neural tissues, with visualization of the LC peripheral to the BMO (Figure 2) especially difficult.^{24,37} The definition of what constitutes a focal LC defect is also important. Defects were required to be greater than $100\mu\text{m}$ in diameter and $30\mu\text{m}$ in depth. The size criteria were chosen to minimize the risk of labeling normal LC pores as defects, to increase inter-

observer agreement, and to allow comparison with previously published results,¹⁵ however, a consequence of these criteria is that small LC defects may have been excluded. In a histological study,³⁸ Jonas and colleagues found that normal LC pores have a mean area of only $4 \mu\text{m}^2$. This suggests that LC defects could be much smaller than the criteria used in the present study. In a pilot study we had attempted to identify LC defects with a diameter of less than $100 \mu\text{m}$ but found poor agreement between graders and the ability to identify small defects to be limited by the resolution of the current EDI-OCT imaging device.

A limitation specific to radial line EDI-OCT scans is that the spacing between the spokes of the scans increases with increasing eccentricity. The definition of a LC defect included the requirement for confirmation of the defect in a neighboring scan, and therefore, due to the orientation of the radial line scans, peripheral LC defects needed to be larger than central LC defects to fulfill this criterion. For example, in Figure 3A there are two possible focal LC defects (arrow heads) present in the radial line EDI-OCT image transecting an inferotemporal RNFL defect. However, in Figure 3B, which shows the radial line scan immediately clockwise to Figure 3A, only one LC defect is present (arrow head). The smaller potential defect in Figure 3A did not meet the requirement for inclusion as a LC defect in the study. If the smaller potential defect had been located more centrally, closer spacing of the radial line scans may have resulted in the defect reaching the criteria for inclusion.

Disinsertion of the peripheral LC has previously been described in glaucomatous eyes using EDI-OCT and it has been suggested that a LC disinsertion is present when, rather than the normal U or W-shaped configuration, there peripheral LC has a downward slope.¹⁵ Due to difficulty visualizing the insertion of the LC peripheral to the BMO, we did not distinguish peripheral LC defects from disinsertions. There was one eye with a possible LC defect peripheral to the BMO, which is shown in Figure 5. An inferotemporal RNFL defect is visible on photography and a peripheral LC defect was thought to be present in a radial line scan transecting the localized RNFL defect (Figure 5A, arrowhead). There was also downward sloping of the peripheral LC in this region, which indicates a possible LC disinsertion according to the classification of Kiumehr and colleagues.¹⁵ The anterior LC had a W-shaped configuration in other regions (Figure 5B).

An important consideration when examining the spatial relationship between focal LC and RNFL defects is the need for accurate alignment of photographs and EDI-OCT images.³⁹⁻⁴¹ In this study we used image-processing software to calculate the degree of misalignment between stereophotographs and EDI-OCT and accounted for this in our analysis. There are, however, limitations of using visible structures such as the optic disc as a reference for localization as the approach is somewhat subjective and different anatomic structures can contribute to the perceived disc margin.³⁰ In contrast, the BMO is a relatively stable landmark identifiable on SD-OCT B-scan images that can be detected using automated algorithms.³⁰ The position of the ONH and fovea relative to a fundus image varies between individuals due to anatomic disparity, and within individuals due to cyclotorsion; however, the location of RNFL bundles remains constant relative to the fovea-BMO center axis.^{30,40,41} The fovea-BMO center axis is therefore a promising tool for image orientation, which could allow measurements to be taken from the same anatomic location.³⁰ We did not use the fovea-BMO axis in the present study as the BMO is not identifiable directly from fundus photographs; however, future imaging devices are likely to incorporate calculation of the fovea-BMO center axis during image acquisition, which is likely to lead to a more precise understanding of the spatial relationships between damaged structures in glaucoma.

Although the present study found a high number of eyes with localized RNFL defects also had a focal LC defect, categorizing eyes, as having diffuse or localized RNFL loss is

somewhat artifactual. For example, eyes with localized RNFL loss often also have diffuse loss, and localized RNFL defects tend to progress by deepening and widening to become diffuse defects.^{29,35,36} It is therefore unsurprising that focal defects of the LC have been reported in glaucomatous eyes with a range of optic disc and visual field abnormalities.¹⁵ Diffuse changes to the LC such as thinning or posterior displacement may also be important and associated with diffuse or localized neural damage.^{5,20,42} Future studies are needed to evaluate the prognostic significance of focal and diffuse LC defects and determine the relationship between change in LC defects and other structural and functional parameters.

In conclusion this study found a high prevalence of focal LC defects in glaucomatous eyes with localized RNFL defects. There was also good spatial correlation between the location of LC defects and the location of RNFL loss suggesting that damage to the LC might contribute to damage to retinal ganglion cell axons. The results of this study add to a growing body of evidence that IOP-related stress damages connective tissue as well as neural tissue.

Acknowledgments

Supported in part by National Institutes of Health/National Eye Institute grants EY021818 (F.A.M.), EY11008 (L.M.Z.), EY14267 (L.M.Z.), EY019869 (L.M.Z.); an unrestricted grant from Research to Prevent Blindness (New York, NY); grants for participants' glaucoma medications from Alcon, Allergan, Pfizer, Merck and Santen.

References

1. Anderson DR. Ultrastructure of human and monkey lamina cribrosa and optic nerve head. *Arch Ophthalmol.* 1969; 82:800–814. [PubMed: 4982225]
2. Wilczek M. The lamina cribrosa and its nature. *Br J Ophthalmol.* 1947; 31:551–565. [PubMed: 18170379]
3. Fechtner RD, Weinreb RN. Mechanisms of optic nerve damage in primary open angle glaucoma. *Surv Ophthalmol.* 1994; 39:23–42. [PubMed: 7974188]
4. Dai C, Khaw PT, Yin ZQ, et al. Structural basis of glaucoma: the fortified astrocytes of the optic nerve head are the target of raised intraocular pressure. *Glia.* 2012; 60:13–28. [PubMed: 21948238]
5. Burgoyne CF, Downs JC, Bellezza AJ, et al. The optic nerve head as a biomechanical structure: a new paradigm for understanding the role of IOP-related stress and strain in the pathophysiology of glaucomatous optic nerve head damage. *Prog Retin Eye Res.* 2005; 24:39–73. [PubMed: 1555526]
6. Quigley HA, Addicks EM, Green WR, Maumenee AE. Optic nerve damage in human glaucoma. II. The site of injury and susceptibility to damage. *Arch Ophthalmol.* 1981; 99:635–649. [PubMed: 6164357]
7. Quigley HA, Hohman RM, Addicks EM, et al. Morphologic changes in the lamina cribrosa correlated with neural loss in open-angle glaucoma. *Am J Ophthalmol.* 1983; 95:673–691. [PubMed: 6846459]
8. Bellezza AJ, Rintalan CJ, Thompson HW, et al. Deformation of the lamina cribrosa and anterior scleral canal wall in early experimental glaucoma. *Invest Ophthalmol Vis Sci.* 2003; 44:623–637. [PubMed: 12556392]
9. Quigley HA, Addicks EM. Chronic experimental glaucoma in primates. II. Effect of extended intraocular pressure elevation on optic nerve head and axonal transport. *Invest Ophthalmol Vis Sci.* 1980; 19:137–152. [PubMed: 6153173]
10. Levy NS, Crapps EE. Displacement of optic nerve head in response to short-term intraocular pressure elevation in human eyes. *Arch Ophthalmol.* 1984; 102:782–796. [PubMed: 6721773]
11. Yang H, Downs JC, Girkin C, et al. 3-D histomorphometry of the normal and early glaucomatous monkey optic nerve head: lamina cribrosa and peripapillary scleral position and thickness. *Invest Ophthalmol Vis Sci.* 2007; 48:4597–4607. [PubMed: 17898283]
12. Sigal IA, Flanagan JG, Tertinegg I, Ethier CR. Predicted extension, compression and shearing of optic nerve head tissues. *Exp Eye Res.* 2007; 85:312–322. [PubMed: 17624325]

13. Quigley HA, Addicks EM. Regional differences in the structure of the lamina cribrosa and their relation to glaucomatous optic nerve damage. *Arch Ophthalmol.* 1981; 99:137–143. [PubMed: 7458737]
14. Sigal IA, Ethier CR. Biomechanics of the optic nerve head. *Exp Eye Res.* 2009; 88:799–807. [PubMed: 19217902]
15. Kiumehr S, Park SC, Syril D, et al. In vivo evaluation of focal lamina cribrosa defects in glaucoma. *Arch Ophthalmol.* 2012; 130:552–559. [PubMed: 22232364]
16. Radius RL. Regional specificity in anatomy at the lamina cribrosa. *Arch Ophthalmol.* 1981; 99:478–486. [PubMed: 7213169]
17. Roberts MD, Liang Y, Sigal IA, et al. Correlation between local stress and strain and lamina cribrosa connective tissue volume fraction in normal monkey eyes. *Invest Ophthalmol Vis Sci.* 2010; 51:295–307. [PubMed: 19696175]
18. Spaide RF, Koizumi H, Pozonni MC. Enhanced depth imaging spectral-domain optical coherence tomography. *Am J Ophthalmol.* 2008; 146:496–500. [PubMed: 18639219]
19. Park SC, De Moraes CG, Teng CC, et al. Enhanced depth imaging optical coherence tomography of deep optic nerve complex structures in glaucoma. *Ophthalmology.* 2012; 119:3–9. [PubMed: 21978593]
20. Lee EJ, Kim TW, Weinreb RN, Kim H. Reversal of lamina cribrosa displacement after intraocular pressure reduction in open-angle glaucoma. *Ophthalmology.* 2013; 120:553–559. [PubMed: 23218823]
21. Lee EJ, Kim TW, Weinreb RN, et al. Visualization of the lamina cribrosa using enhanced depth imaging spectral-domain optical coherence tomography. *Am J Ophthalmol.* 2011; 152:87–95. [PubMed: 21570046]
22. Lee EJ, Kim TW, Weinreb RN, et al. Three-dimensional evaluation of the lamina cribrosa using spectral domain optical coherence tomography in glaucoma. *Invest Ophthalmol Vis Sci.* 2012; 53:198–204. [PubMed: 22167102]
23. Lee EJ, Kim TW, Weinreb RN. Improved reproducibility in measuring the laminar thickness on enhanced depth imaging SD-OCT images using maximum intensity projection. *Invest Ophthalmol Vis Sci.* 2012; 53:7576–7582. [PubMed: 23074212]
24. Inoue R, Hangai M, Kotera Y, et al. Three-dimensional high-speed optical coherence tomography imaging of lamina cribrosa in glaucoma. *Ophthalmology.* 2009; 116:214–222. [PubMed: 19091413]
25. Sample PA, Girkin CA, Zangwill LM, et al. ADAGES Study Group. The African Descent and Glaucoma Evaluation Study (ADAGES): design and baseline data. *Arch Ophthalmol.* 2009; 127:1136–1145. [PubMed: 19752422]
26. Medeiros FA, Vizzeri G, Zangwill LM, et al. Comparison of retinal nerve fiber layer and optic disc imaging for diagnosing glaucoma in patients suspected of having the disease. *Ophthalmology.* 2008; 115:1340–1346. [PubMed: 18207246]
27. Medeiros FA, Weinreb RN, Sample PA, et al. Validation of a predictive model to estimate the risk of conversion from ocular hypertension to glaucoma. *Arch Ophthalmol.* 2005; 123:1351–60. [PubMed: 16219726]
28. Jonas JB, Schiro D. Localised wedge shaped defects of the retinal nerve fibre layer in glaucoma. *Br J Ophthalmol.* 1994; 78:285–290. [PubMed: 8199115]
29. Leung CK, Choi N, Weinreb RN, et al. Retinal nerve fiber layer imaging with spectral-domain optical coherence tomography: pattern of RNFL defects in glaucoma. *Ophthalmology.* 2010; 117:2337–2344. [PubMed: 20678802]
30. Chauhan BC, Burgoyne CF. From Clinical Examination of the Optic Disc to Clinical Assessment of the Optic Nerve Head: A Paradigm Change. *Am J Ophthalmol.* 2013; 156:218–227. [PubMed: 23768651]
31. Cohen J. Weighted kappa: nominal scale agreement provision for scaled disagreement or partial credit. *Psychol Bull.* 1968; 70:213–220. [PubMed: 19673146]
32. Landis JR, Koch GG. The measurement of observer agreement for categorical data. *Biometrics.* 1977; 33:159–164. [PubMed: 843571]

33. Leung CK, Yu M, Weinreb RN, et al. Retinal nerve fiber layer imaging with spectral-domain optical coherence tomography: a prospective analysis of age-related loss. *Ophthalmology*. 2012; 119:731–737. [PubMed: 22264886]
34. Strouthidis NG, Grimm J, Williams GA, et al. A comparison of optic nerve head morphology viewed by spectral domain optical coherence tomography and by serial histology. *Invest Ophthalmol Vis Sci*. 2010; 51:1464–1474. [PubMed: 19875649]
35. Hoyt WF, Newman NM. The earliest observable defect in glaucoma? *Lancet*. 1972; 1:692–699. [PubMed: 4125199]
36. Sommer A, Miller NR, Pollack I, et al. The nerve fiber layer in the diagnosis of glaucoma. *Arch Ophthalmol*. 1977; 95:2149–2156. [PubMed: 588106]
37. Kagemann L, Ishikawa H, Wollstein G, et al. Ultrahigh-resolution spectral domain optical coherence tomography imaging of the lamina cribrosa. *Ophthalmic Surg Lasers Imaging*. 2008; 39(suppl):S126–S131. [PubMed: 18777881]
38. Jonas J, Mardin CY, Schlötzer-Schrehardt U, Naumann GO. Morphometry of the human lamina cribrosa surface. *Invest Ophthalmol Vis Sci*. 1991; 32:401–415. [PubMed: 1993592]
39. Garway-Heath DF, Poinosawmy D, Fitzke FW, Hitchings RA. Mapping the visual field to the optic disc in normal tension glaucoma eyes. *Ophthalmology*. 2000; 107:1809–1815. [PubMed: 11013178]
40. Jansonius NM, Nevalainen J, Selig B, Zangwill LM, Sample PA, Budde WM, Jonas JB, Lagreze WA, Airaksinen PJ, Vonthein R, Levin LA, Paetzold J, Schiefer U. A mathematical description of nerve fiber bundle trajectories and their variability in the human retina. *Vision Res*. 2009; 49:2157–2163. [PubMed: 19539641]
41. Hood DC, Raza AS, de Moraes CG, Liebmann JM, Ritch R. Glaucomatous damage of the macula. *Prog Retin Eye Res*. 2013; 32:1–21. [PubMed: 22995953]
42. Reis AS, O'Leary N, Stanfield MJ, et al. Lamina displacement and prelaminar tissue thickness change after glaucoma surgery imaged with optical coherence tomography. *Invest Ophthalmol Vis Sci*. 2012; 53:5819–5826. [PubMed: 22807291]

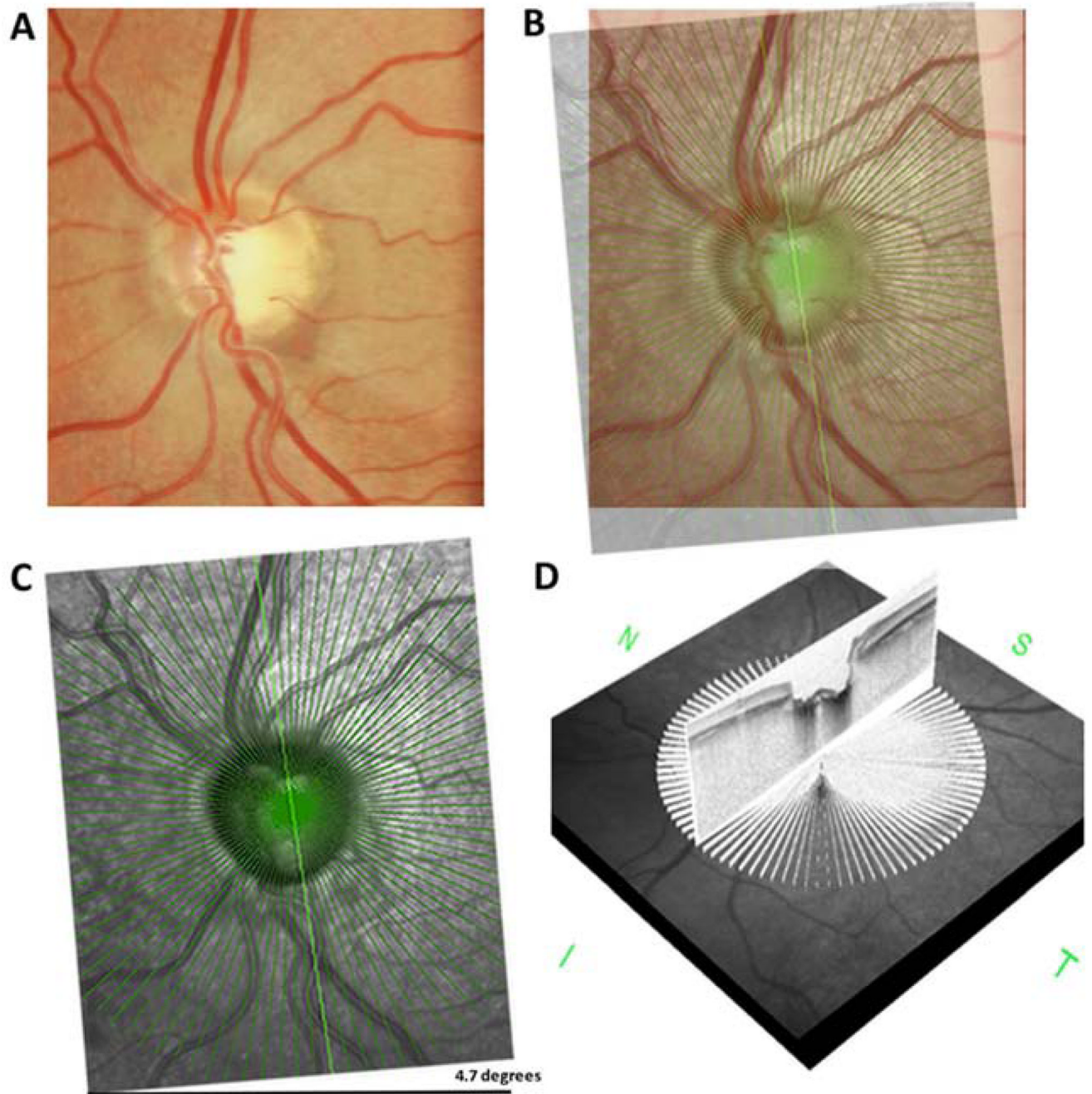


Figure 1. Optic disc photograph of an eye with an inferior localized retinal nerve fiber layer (RNFL) defect (A). The infrared en face radial line enhanced depth optical coherence tomography (EDI-OCT) image for the same eye was superimposed on the optic disc photograph, with 4.7 degrees of rotation required for alignment (B–C). Each of the 48 radial line EDI-OCT images were examined for lamina cribrosa defects (D).

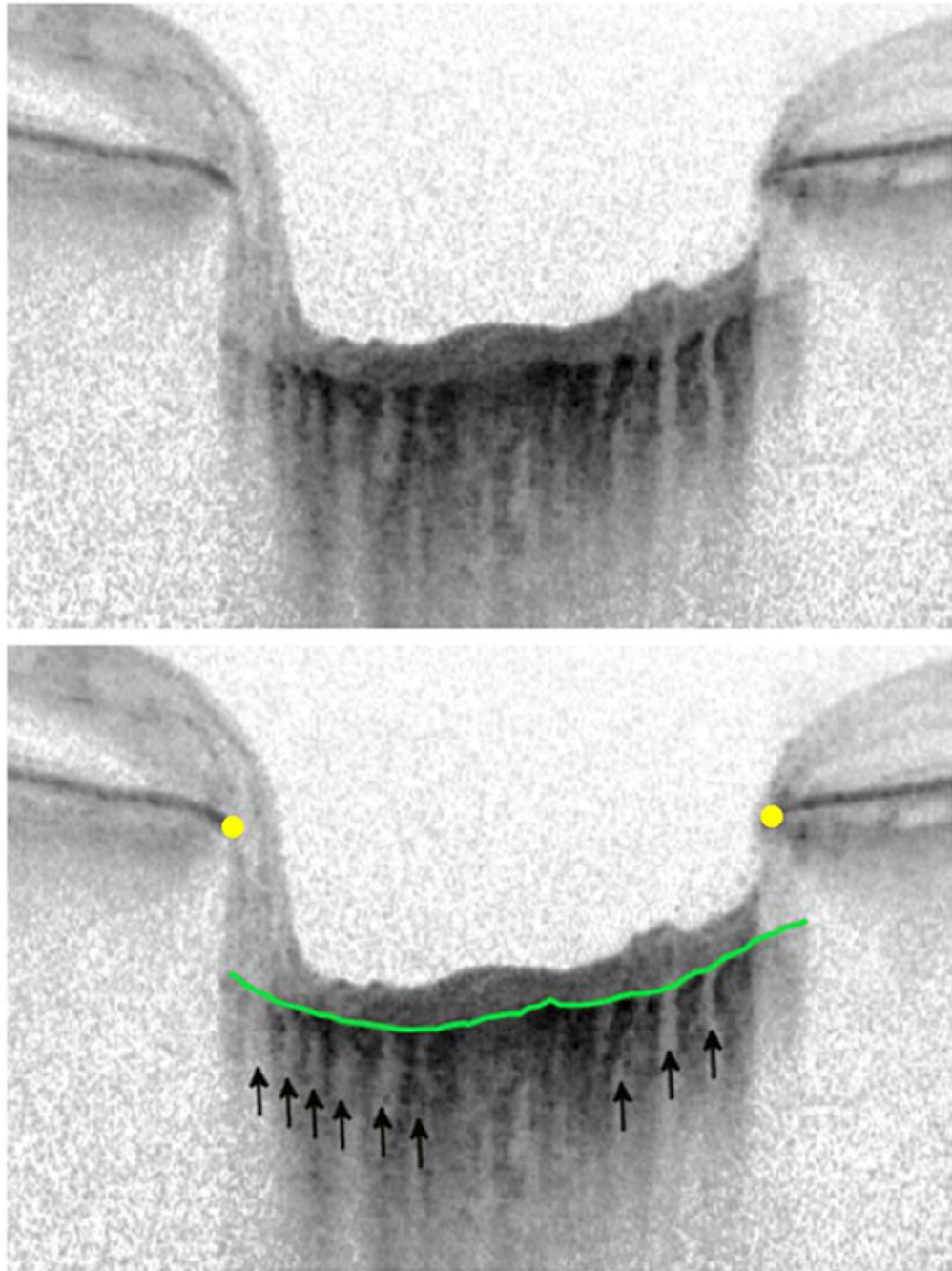


Figure 2. Image of lamina cribrosa without a focal lamina cribrosa defect. There are multiple small full thickness lamina perforations (<100 microns in diameter) likely corresponding to lamina pores (arrows). The anterior lamina surface is indicated by the green line and the Bruch's membrane terminations by the yellow dots.

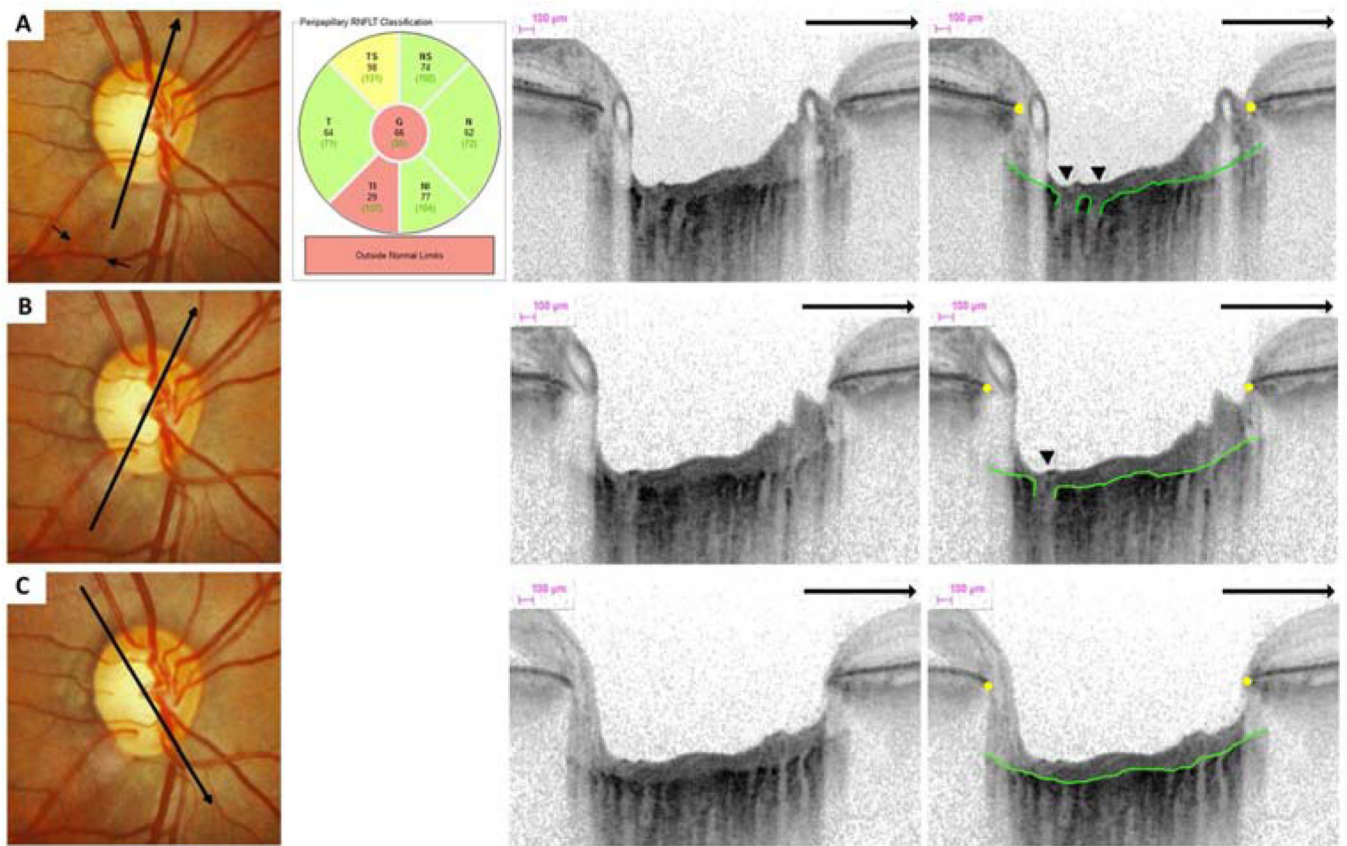


Figure 3. Optic disc photographs, retinal nerve fiber layer (RNFL) thickness classification and multiple enhanced depth optical coherence tomography (EDI-OCT) radial scans of the same eye. An inferior-temporal RNFL defect is visible on optic disc photographs (small arrows). There is a lamina cribrosa (LC) defect on two neighboring radial EDI-OCT (arrow head) scans (A–B) in the same sector as the RNFL defect. The EDI-OCT radial scan direction is indicated (large arrows). LC defects were not visible in other regions (C).

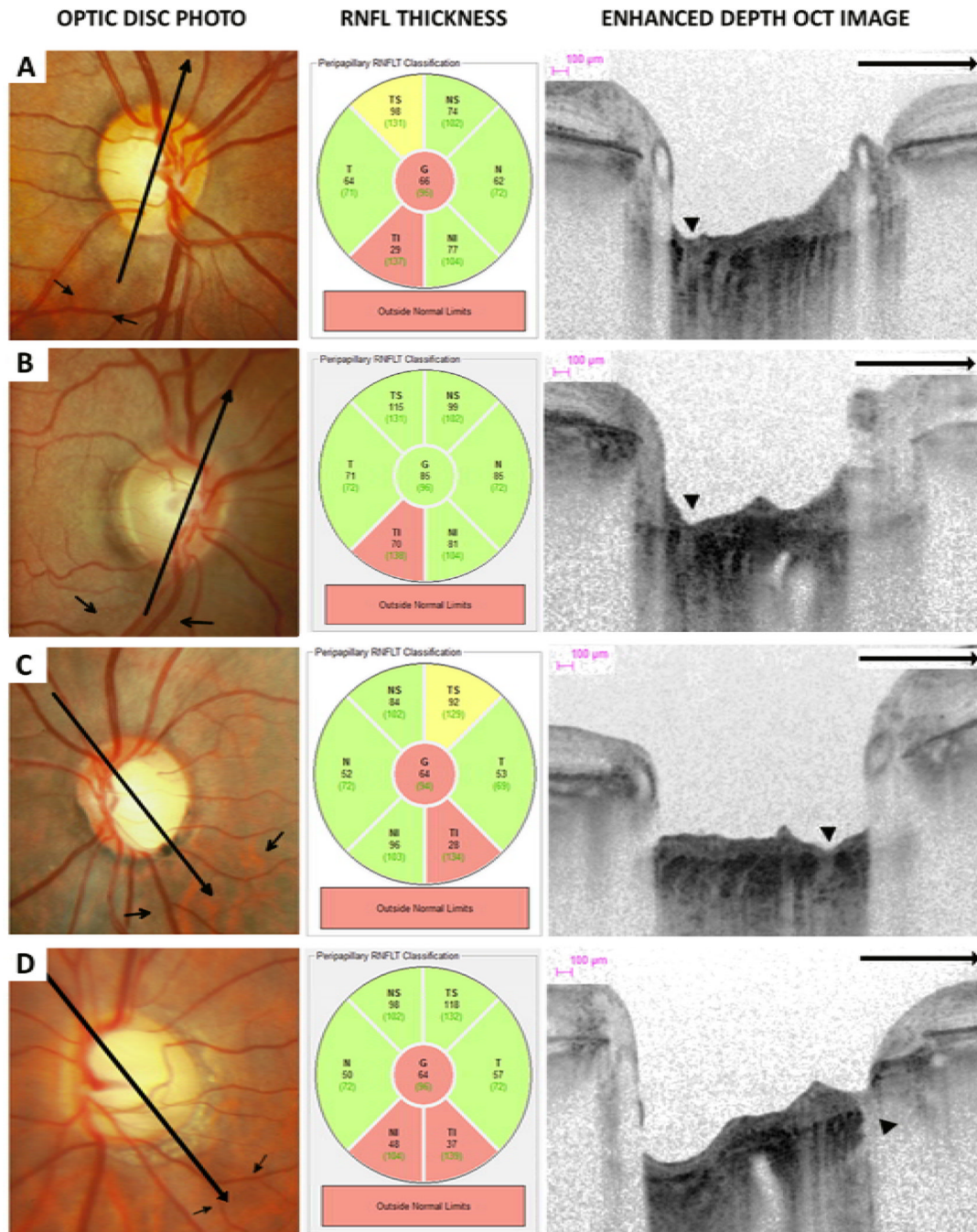


Figure 4. Optic disc photographs, retinal nerve fiber layer (RNFL) thickness classification and multiple enhanced depth optical coherence tomography (EDI-OCT) radial scans of eyes with lamina cribrosa defects (arrow heads) corresponding to areas of localized RNFL loss (small arrows). The EDI-OCT radial scan direction is indicated (large arrows).

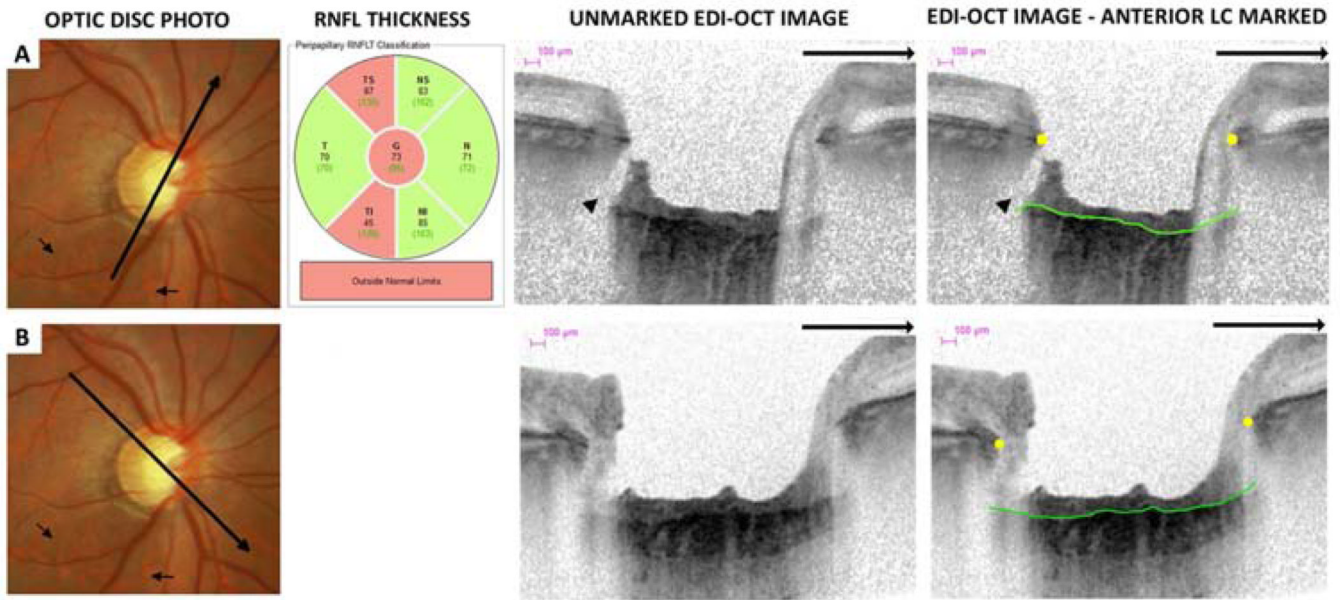


Figure 5.

Optic disc photographs, retinal nerve fiber layer (RNFL) thickness classification and multiple enhanced depth optical coherence tomography (EDI-OCT) radial scans of an eye with a peripheral lamina cribrosa (LC) defect. An inferior-temporal retinal nerve fiber layer defect was identified on optic disc photographs (small arrows) and a corresponding peripheral LC defect on EDI-OCT (arrow heads) (A). The EDI-OCT radial scan direction is indicated (large arrows). The anterior border of the lamina cribrosa (green line) and terminations of Bruch's membrane (yellow dots) are highlighted in the marked EDI-OCT image. There were no LC defects detected in other locations, including in the superior-temporal sector where RNFL thinning was also detected by OCT (B).

Table 1

Demographic and clinical characteristics of healthy subjects and those with localized retinal nerve fiber layer (RNFL) defects.

	RNFL defect N= 20 eyes, 14 subjects	Healthy N= 40 eyes, 25 subjects	P value
Age (years)	67.3 +/- 9.7	67.6 +/- 10.1	0.95 [†]
Gender	7 (50%) Female	15 (60%) Female	0.74 [‡]
Race	10 White 4 African American	15 White 10 African American	0.73 [‡]
CCT (µm)	526 +/- 39	234 +/- 44	0.53 [†]
Axial length (mm)	24.1 (23.2 to 24.9)	23.9 (23.5 to 24.7)	0.86 [*]
Mean deviation (dB)	-4.8 +/- 2.9	0.2 +/- 1.3	<0.001 [†]
RNFL thickness (µm)	72.8 +/- 11.2	94.6 +/- 9.3	<0.001 [†]
Eyes with LC defects	15 (75%)	1 (3%)	<0.001 [‡]

[†] mean +/- standard deviation, t-test

[‡] Fishers exact test

^{*} median (interquartile range), Wilcoxon test

CCT – central corneal thickness, LC – lamina cribrosa